

Superfluid, Supersolid, and Checkerboard Solid in Two-Component Bosons in an Optical Lattice: Study by Means of Gross-Pitaevskii Theory and Monte - Carlo Simulations

Yoshihito Kuno, Keita Suzuki, and Ikuo Ichinose

Department of Applied Physics, Nagoya Institute of Technology, Nagoya 466-8555, Japan

The bosonic t-J model is a strong-on-site repulsion limit of the two-component Bose-Hubbard model and is expected to be realized by experiments of cold atoms in an optical lattice. In previous papers, we studied the bosonic t-J model by both analytical methods and numerical Monte - Carlo (MC) simulations. However, in the case of finite J_z , where J_z is the z -component coupling constant of the pseudospin interaction, the phase diagram of the model was investigated by assuming the checkerboard type of boson densities. In this study, we shall continue our previous study of the bosonic t-J model using both the Gross-Pitaevskii (GP) theory and MC simulations without assuming any pattern of boson densities. These two methods complement each other and give reliable results. We show that as J_z is increased, the superfluid state evolves into a supersolid (SS), and furthermore into a genuine solid with the checkerboard symmetry. In the present study, we propose a method identifying quantum phase transitions in the GP theory. We also study finite-temperature phase transitions of the superfluidity and the diagonal solid order of the SS by MC simulations.

1. Introduction

Cold atomic gases in an optical lattice (OL) are one of the most actively studied systems these days because of their versatility.¹⁾ Sometimes they are regarded as a “quantum simulator”, e.g., for the strongly-correlated many-body systems as they are highly controllable.²⁾ The dimension and type of OL are controlled by adjusting the experimental apparatus, the interactions between atoms are freely controlled by the Feshbach resonance and using dipolar bosons etc.³⁾

It is now widely accepted that the physical properties of the system of bosonic cold atomic gases in OL are well-described by the Bose-Hubbard model.⁴⁾ From the viewpoint of the strongly-correlated electron systems such as the high- T_C superconducting (SC) materials, the two-component Bose-Hubbard model with the strong on-site repulsion is one of the most

interesting systems. Closely related systems can be realized by experiments on boson gases, e.g., ^{85}Rb - ^{87}Rb and ^{87}Rb - ^{41}K mixtures.^{5,6)} As in the cuprates, it is expected that a pseudospin long-range order (LRO) appears at low temperature. Besides that magnetic order, a superfluid (SF) is also expected to form at finite hole doping. In general, the competition between the (antiferromagnetic) magnetic order and the superfluidity takes place, and then the system exhibits an interesting phase diagram.

In our previous papers,^{7,8)} we showed that the strong on-site repulsion limit of the Bose-Hubbard model is described by the bosonic t-J model.⁹⁾ We also discussed there that the bosonic t-J model appears from models similar to a bosonic counterpart of the d-p model for the strongly-correlated electron systems. It is expected that a bosonic counterpart of the electronic d-p system will be realized in the near future by experiments on Bose gas systems in the two-dimensional Lieb lattice. It should be remarked that, in the bosonic t-J model as an effective low-energy model of the bosonic d-p model, the parameters t and J are controlled almost freely in contrast to the case of the cuprates.

Using both analytical and numerical methods, we investigated the phase diagram of the bosonic t-J model in the previous studies.^{7,8)} For numerical Monte-Carlo (MC) simulations, we assumed a homogeneous or checkerboard (CB) configuration for boson densities. Amplitude modes of the bosons are then integrated out analytically, and a quantum MC simulation was performed for the resultant effective model for the phase degrees of freedom of the boson fields. Then, we obtained the phase diagram of the bosonic t-J model.

In the present study, we shall continue the above studies and investigate the phase diagram of the bosonic t-J model *without assuming any density pattern of the bosons*. We employ both the Gross-Pitaevskii (GP) theory and quantum MC simulations, in which the densities of bosons are treated as dynamical variables. The both methods are used to study the groundstate properties of the system with Bose-Einstein condensation (BEC) and complement with each other. In the present paper, we propose a method of identifying phase transitions in the GP theory, which is found with the help of the MC simulation.

This paper is organized as follows. In Sec.2, we introduce an extended version of the bosonic t-J model. The GP equations and MC simulation for the bosonic t-J model are explained in detail. Section 3 is the main body of the present paper. Numerical results of the GP equations and MC simulation are given. We shall focus on the phase in which both bosons form BEC, i.e., the 2SF state, and study how this state evolves as the antiferromagnetic (AF) coupling J_z is increased. In the first subsection, results of the GP equations are shown. The phase transition from the 2SF to a supersolid (SS) is observed at some critical value of the

AF coupling by studying density snapshots and correlation functions. As the AF coupling is increased further, the transition from the SS to a genuine solid without the SF long-range order (LRO) takes place. In the second and third subsections, results of the MC simulation are given. Calculations of the internal energy and its quantum fluctuation, which are in good agreement with those of the GP equations, are shown, and the properties of observed phase transitions are discussed. In the fourth subsection, finite-temperature (T) phase structures of the SS and CB solid are investigated by the MC simulations. As T increases, the CB solid order disappears first and then the long-range SF order does at a higher T . Section 4 is devoted to the conclusion.

2. Models: Bosonic t-J model and GP theory for two-component atoms

As we explained in the introduction, we shall study the extended t-J model on a square lattice whose Hamiltonian is given as

$$H_{\text{EIJ}} = H_{\text{IJ}} + H_V, \quad (1)$$

$$H_{\text{IJ}} = - \sum_{\langle i,j \rangle} (t_a a_i^\dagger a_j + t_b b_i^\dagger b_j + \text{h.c.}) - J_{xy} \sum_{\langle i,j \rangle} (S_i^x S_j^x + S_i^y S_j^y) + J_z \sum_{\langle i,j \rangle} S_i^z S_j^z, \quad (2)$$

$$H_V = \frac{V_0}{4} \sum_i \left((a_i^\dagger a_i - \rho_{ai})^2 + (b_i^\dagger b_i - \rho_{bi})^2 \right), \quad (3)$$

where a_i^\dagger and b_i^\dagger are boson creation operators at site i of the square lattice and t_a and t_b are the hopping parameters. The pseudospin operator \vec{S}_i is given as $\vec{S}_i = \frac{1}{2} B_i^\dagger \vec{\sigma} B_i$ with $B_i = (a_i, b_i)^t$, and $\vec{\sigma}$ is the Pauli spin matrix. In the t-J model, the doubly-occupied state is excluded at each site as it is derived from the Bose-Hubbard model in the strong on-site repulsion limit. We add the on-site repulsive terms H_V of the Hubbard type, which control fluctuations in the number of the particles at each site, although it is expected that this term substantially appears from the effects of the terms in H_{IJ} in Eq.(2), particularly the J -terms. For more details, see later discussion on the relationship between the extended t-J model and the GP theory. Then, in H_V , V_0 is a positive parameter and $\rho_{ai} + \rho_{bi} \leq 1$. To impose the local constraint $a_i^\dagger a_i + b_i^\dagger b_i < 1$ on the physical state in the Hilbert space, the *slave-particle representation* is useful.

In our previous paper,⁷⁾ we studied the phase diagram of the model H_{EIJ} by the MC simulations in the slave-particle representation. The case of $J_z \ll 1$ can be studied straightforwardly as the integration over the amplitude modes of the bosons a_i and b_i can be carried out without any difficulties, and the action of the resultant model of the phase degrees of freedom is positive-definite. We call the resultant model the extended XY model.

On the other hand, the case of finite J_z has been investigated in Ref.8. In that study, we

focused on the appearance of the CB-type density pattern of the bosons and found that a SS state forms for intermediate values of J_z although for a large J_z the genuine CB solid without the SF appears as the groundstate. In that study, we assumed the density pattern such as $\rho_{a \text{ even-site}} = \rho_{b \text{ odd-site}}$ and $\rho_{a \text{ odd-site}} = \rho_{b \text{ even-site}}$, and therefore the considered states have the translational symmetry of the twofold lattice spacing.

In the present research, we also study a GP theory for a system of two-component bosons trapped in an OL, which is regarded as a genuine system in experiments for the t-J model on the lattice. In that study, we do not assume any translational symmetry for solutions. It will become clear that the results of the GP equations are helpful for performing reliable MC simulations for the t-J model.

We use the continuum description of the system and introduce the following periodic potential in the GP equations to simulate the square OL, i.e.,

$$V_{\text{OL}} = A_{\text{OL}} \left(\sin^2(\pi x/\ell) + \sin^2(\pi y/\ell) \right), \quad (4)$$

where the positive parameter A_{OL} is the depth of the OL and ℓ is the lattice spacing, which are determined by the strength and wavelength of the laser used in experiments, respectively. See Fig.1. By using the OL potential Eq.(4), Hamiltonian of the a and b atoms is given as

$$H_{\text{GP}} = \int d^2x \left[\sum_{\alpha=a,b} \psi_{\alpha}^{\dagger} \left(-\frac{\hbar^2}{2m} \nabla^2 + V_{\text{OL}} \right) \psi_{\alpha} - g_{aa} |\psi_a|^2 (1 - |\psi_a|^2) - g_{bb} |\psi_b|^2 (1 - |\psi_b|^2) + g_{ab} |\psi_a|^2 |\psi_b|^2 \right], \quad (5)$$

where g_{aa} 's are the intra- and inter-repulsive coupling constants. In the present study, we mostly consider the case $g_{aa} = g_{bb} > g_{ab}$ in which two atoms are miscible.

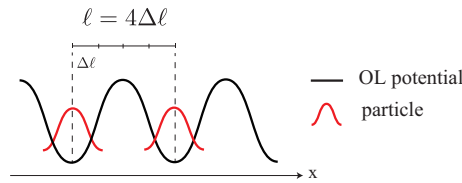


Fig. 1. (Color online) Optical lattice described by the potential V_{OL} in Eq.(4). Long-range interactions between atoms in adjacent minima of OL are given by Eq.(6). $\Delta\ell$ is the spatial slice used for solving the GP equations.

The Hamiltonian H_{GP} in Eq.(5) describes the system of two-component BEC in the OL and with the intra- and inter-species on-site repulsive interactions. Then, we add the following long-range interactions between atoms to the Hamiltonian of the GP theory, which

corresponds to the J -terms in the t-J model H_{tJ} ,

$$H_{\text{LR}} = \int d^2x \mathcal{H}_{\text{LR}},$$

$$\mathcal{H}_{\text{LR}} = \sum_{|x-y|=\ell} \left[-j_{xy} \psi_a^\dagger(x) \psi_b(x) \psi_a(y) \psi_b^\dagger(y) + \text{H.c.} \right. \\ \left. + j_z (|\psi_a(x)|^2 - |\psi_b(x)|^2)(|\psi_a(y)|^2 - |\psi_b(y)|^2) \right], \quad (6)$$

where j_{xy} and j_z are parameters corresponding to J_{xy} and J_z , respectively, and $|x - y| = \ell$ denotes that the distance between sites x and y is ℓ . See Fig.1. Then, the total Hamiltonian $H_{\text{GP}} + H_{\text{LR}}$ gives the following GP equations:¹⁰⁾

$$(i - \gamma)\hbar \frac{\partial \psi_a}{\partial t} = \left[-\frac{\hbar^2}{2m} \nabla^2 + V_{\text{OL}} + g_{aa} |\psi_a|^2 + g_{ab} |\psi_b|^2 - \mu \right] \psi_a \\ + \sum_{y, |x-y|=\ell} \left[-j_{xy} \psi_b^*(x) \psi_b(y) \psi_a(y) + j_z \psi_a(x) (|\psi_a(y)|^2 - |\psi_b(y)|^2) \right],$$

$$(i - \gamma)\hbar \frac{\partial \psi_b}{\partial t} = \left[-\frac{\hbar^2}{2m} \nabla^2 + V_{\text{OL}} + g_{bb} |\psi_b|^2 + g_{ba} |\psi_a|^2 - \mu \right] \psi_b \\ + \sum_{y, |x-y|=\ell} \left[-j_{xy} \psi_a^*(x) \psi_a(y) \psi_b(y) + j_z \psi_b(x) (|\psi_b(y)|^2 - |\psi_a(y)|^2) \right], \quad (7)$$

where μ is the chemical potential and γ is a phenomenological dissipative damping parameter. In the practical calculation, we set $\gamma = 0.1$, for which the convergence of solutions is obtained most smoothly in the time evolution of the GP equations, although its value does not substantially affect the physical results. We think that this result comes from the fact that *we are studying stationary states in a system with stable low-energy states*. For the study of a system in an external magnetic field (an effective magnetic field can be generated by rotating boson gas systems), which was discussed in Ref.10 etc, a smaller γ has to be used to obtain reliable results, as the system exhibits nontrivial dynamical behaviors by the appearance of vortices etc.

In a practical numerical calculation, we first turn off H_{LR} to verify that bosons tend to locate in the minima of the OL, and then turn on H_{LR} to see the effects of the j -terms. The differential equations in Eq.(7) are converted to difference equations as $\frac{\partial \psi}{\partial x} \Rightarrow (\psi(x + \Delta\ell) - \psi(x))/\Delta\ell$, where the spatial slice $\Delta\ell$ is taken as $\Delta\ell = \ell/4$ and is set to unity in the calculation, $\Delta\ell = 1$. Then, $\ell = 4$ in this unit. See Fig.1. Similarly, the time slice Δt is used as $\frac{\partial \psi}{\partial t} \Rightarrow (\psi(t + \Delta t) - \psi(t))/\Delta t$ and is set to $\Delta t = 10^{-4}$ in the numerical study. Natural unit of time is $\frac{2m(\Delta\ell)^2}{\hbar}$ and it is estimated as $\frac{2m(\Delta\ell)^2}{\hbar} \sim (10^{-5} - 10^{-4})$ s for typical experiments. From this observation, we used the value $\Delta t = 10^{-4}$. We have verified the stability of the obtained solutions of the GP equations as varying values of Δt and γ , such as $\Delta t = 10^{-5}$ and $\gamma = 0.05$.

It is instructive to compare the above GP equations to those of the t-J model derived from Eqs.(1), (2) and (3),

$$\begin{aligned}
(i - \gamma)\hbar \frac{\partial a_i}{\partial t} &= -t_a \sum_{j \in iNN} a_j - 2J_{xy} \sum_{j \in iNN} b_i a_j b_j^\dagger + J_z \sum_{j \in iNN} a_i (a_j^\dagger a_j - b_j^\dagger b_j) \\
&\quad + \frac{V_0}{2} a_i (a_i^\dagger a_i - \rho_{ai}), \\
(i - \gamma)\hbar \frac{\partial b_i}{\partial t} &= -t_b \sum_{j \in iNN} b_j - 2J_{xy} \sum_{j \in iNN} a_i b_j a_j^\dagger - J_z \sum_{j \in iNN} b_i (a_j^\dagger a_j - b_j^\dagger b_j) \\
&\quad + \frac{V_0}{2} b_i (b_i^\dagger b_i - \rho_{bi}),
\end{aligned} \tag{8}$$

where $j \in iNN$ stands for the nearest-neighbor (NN) sites of i . We identify the lattice spacing of the OL $\ell \sim a_L$, where a_L is the lattice spacing of the square lattice on which the t-J model is defined. As $[\psi] = (\text{dimension of } \psi) = (\text{length})^{-1}$ and $[a] = [b] = (\text{length})^0$, we have $\psi_\alpha \sim \alpha/\ell$ ($\alpha = a, b$). Then, the following straightforward correspondence between the parameters in the two systems is obtained:

$$j_{xy} \sim 2J_{xy}/\ell^2, \quad j_z \sim J_z/\ell^2, \quad g_{aa} = g_{bb} \sim V_0/(2\ell^2). \tag{9}$$

However, a practical calculation shows that the nonlocal j -terms (J -terms) strongly suppress the density fluctuations of atoms at each site. See for example, Fig.2. Therefore, H_V in the extended t-J model acquires the renormalization effect from the J -terms and can be regarded as the leading term.

Finally, let us briefly explain the MC simulation of the t-J model described by the slave-particle representation,⁷⁾

$$a_i = \phi_i^\dagger \varphi_{i1}, \quad b_i = \phi_i^\dagger \varphi_{i2}, \tag{10}$$

$$(\phi_i^\dagger \phi_i + \varphi_{i1}^\dagger \varphi_{i1} + \varphi_{i2}^\dagger \varphi_{i2} - 1)|\text{Phys}\rangle = 0, \tag{11}$$

where ϕ_i is a boson operator that *annihilates hole* at site i , whereas φ_{1i} and φ_{2i} are bosons that represent the pseudospin degrees of freedom. $|\text{Phys}\rangle$ is the physical state of the slave-particle Hilbert space. Then, the partition function is given by the path-integral formalism as

$$\begin{aligned}
Z &= \int [D\phi D\varphi_1 D\varphi_2] \exp \left[- \int d\tau \left(\bar{\varphi}_{1i}(\tau) \partial_\tau \varphi_{1i}(\tau) \right. \right. \\
&\quad \left. \left. + \bar{\varphi}_{2i}(\tau) \partial_\tau \varphi_{2i}(\tau) + \bar{\phi}_i(\tau) \partial_\tau \phi_i(\tau) + H_{\text{EJ}} \right) \right],
\end{aligned} \tag{12}$$

where τ is the imaginary time, H_{EJ} is expressed by the slave particles, and the above path integral is calculated under the constraint given by Eq.(11). Before performing the MC sim-

ulation, we parameterize φ 's and ϕ as ($\sum_{a=1,2,3} \rho_{ai} = 1$)

$$\varphi_{1i} = \sqrt{\rho_{1i} + \ell_{1i}} \exp(i\omega_{1i}), \quad \varphi_{2i} = \sqrt{\rho_{2i} + \ell_{2i}} \exp(i\omega_{2i}), \quad \phi_i = \sqrt{\rho_{3i} + \ell_{3i}} \exp(i\omega_{3i}), \quad (13)$$

and integrate out the radial degrees of freedom controlled by the term H_V . The constraint $\ell_{1i} + \ell_{2i} + \ell_{3i} = 0$ can be incorporated by using a Lagrange multiplier $\lambda_i(\tau)$. The variables $\ell_{\sigma i}$ ($\sigma = 1, 2, 3$) also appear in H_U , but we ignore them by simply replacing $\varphi_{\sigma i} \rightarrow \sqrt{\rho_{\sigma i}} \exp(i\omega_{\sigma i})$, and then we have

$$\int d\lambda_i d\ell_i e^{\int d\tau \sum_{\sigma=1}^3 (-V_0(\ell_{\sigma i})^2 + i\ell_{\sigma i}(\partial_\tau \omega_{\sigma i} + \lambda_i))} = \int d\lambda_i e^{-\frac{1}{4V_0} \int d\tau \sum_{\sigma} (\partial_\tau \omega_{\sigma i} + \lambda_i)^2}. \quad (14)$$

The resultant quantity on the RHS of Eq.(14) is positive-definite, and therefore the numerical study by the MC simulation can be carried out without any difficulty. It should be remarked that the Lagrange multiplier λ_i in Eq.(14) behaves as a gauge field, i.e., the RHS of Eq.(14) is invariant under the following ‘‘gauge transformation’’, $\omega_{\sigma i} \rightarrow \omega_{\sigma i} + \alpha_i$, $\lambda_i \rightarrow \lambda_i - \partial_\tau \alpha_i$.

The partition function Z in Eq.(12) depends on the local density of the bosons ρ_{ai} . In the previous studies, we assumed a homogeneous distribution of bosons in the case of $J_z \ll 1$ or the CB symmetry for a finite J_z and treated the *global density difference* $\Delta\rho \equiv \rho_{\text{1even-site}} - \rho_{\text{1odd-site}} = -(\rho_{\text{2even-site}} - \rho_{\text{2odd-site}})$ as a variational parameter. These treatments obviously preclude the possibility of, for example., a phase-separated state. In the present study, we shall treat the *local densities* ρ_{ai} as variation variables and determine them using the requirement of the minimum free-energy condition. This means that not only the V -term in H_V but also the t and J -terms affect the local density of the bosons. Numerical studies in Sec.3 show that the homogeneous or the CB configuration of the boson density dominates in most of the parameter regions of the models as we assumed in our previous study.⁸⁾

3. Numerical results: Solutions to GP theory and MC simulation of t-J model

In this section, we shall show the results obtained by the numerical calculations. We first show numerical solutions of the GP equations. We start with the state with the BECs of both the a and b atoms and then we increase j_z and see how the state evolves. Solutions of the GP equation show that a SS appears at some critical value of j_z . As j_z is increased further, the BECs disappear, and the genuine solid with only the CB order replaces the SS. In the second and third subsections of this section, we show the results of the MC simulations. We first consider the case of an equal-mass $t_a = t_b = t$, and show that the results are in good agreement with those of the GP equations. Calculations of the correlation functions by the MC simulations identify unambiguously existing orders in each phase. Then, we apply a similar MC analysis in the case of a different mass such as $t_a = 2t_b$, and clarify the phase

diagram. Finally, in the last subsection, we study the finite-temperature phase diagram of the SS and CB solid and see how two orders, i.e., the SF and CB, disappear by the thermal fluctuations as the temperature increases. All the calculations were carried out for the system at a filling factor 0.35 for each atom (therefore, the total filling factor is 0.7).

3.1 Gross-Pitaevskii theory

In this subsection, we shall show solutions of the GP equations in Eq.(7). We started with the case of $j_z = 0$ and increased j_z gradually.¹¹⁾ The depth of the OL was set to $A_{OL} = 2$. For $j_z = 0$, all the bosons are trapped in the OL, and the homogeneous state with the double BECs forms for a sufficiently large $t_h \equiv \frac{\hbar^2}{m(\Delta\ell)^2} = \frac{\hbar^2}{m}$. See the density profiles $|\psi_a(x)|$ and $|\psi_b(x)|$ in Figs.2 and 3. This state corresponds to the 2SF state with the ferromagnetic (FM) pseudo-spin order for $j_{xy} > 0$, which was observed previously in the MC simulations.⁸⁾ By the practical calculation, we verified that for every configuration (except the phase-separated state, see later discussion), a local constraint similar to that of the t-J model is satisfied as

$$\int_{x \in \text{site of OL}} d^2x (|\psi_a(x)|^2 + |\psi_b(x)|^2) \simeq 0.7, \quad (15)$$

where $\int_{x \in \text{site of OL}}$ denotes that the integral over the $(\ell \times \ell)$ region of a single site of the OL. See Fig.2. The average hole density is, therefore, 30% as we explained above. The stability of Eq.(15) is guaranteed by the conservation of the total number of particles in the time evolution of the GP equations.

We started with the above 2SF state and increased j_z to see how the state evolves. We found that the SS appears at a certain critical value j_z , $j_{z1} \simeq 6.0$. There the density difference $|\psi_a(x)|^2 - |\psi_b(x)|^2 \neq 0$ appears, but the phase coherence of the a and b -atoms still exists, as verified by calculating the following correlation functions:

$$F_\alpha(r) = \left\langle \frac{1}{2|\psi_\alpha(x)\psi_\alpha(x+r)|} (\psi_\alpha^*(x)\psi_\alpha(x+r) + \text{c.c.}) \right\rangle, \quad (16)$$

where $\alpha = a, b$, and x and $x+r$ are both sites of the OL. $F_\alpha(r)$ in Eq.(16) was evaluated by substituting the obtained “wave functions” $\{\psi_a(x), \psi_b(x)\}$ after a sufficiently long evolution period in the GP equations. For $j_z = 7$, see Fig.4.

We increased j_z further. At the second critical value of j_z , $j_{z2} \simeq 8.0$, the superfluidity of the atoms is lost and the genuine solid with the CB pattern appears instead of the SS. In Figs.3 and 4, we show snapshots of each phase and also correlation functions in the SS. We also verified that, for a much larger $j_z \gg A_{OL}$ and $1/m$, the phase separation into the region of the pure CB solid and the hole-rich region takes place, i.e., *Eq.(15) is not satisfied in that state.*

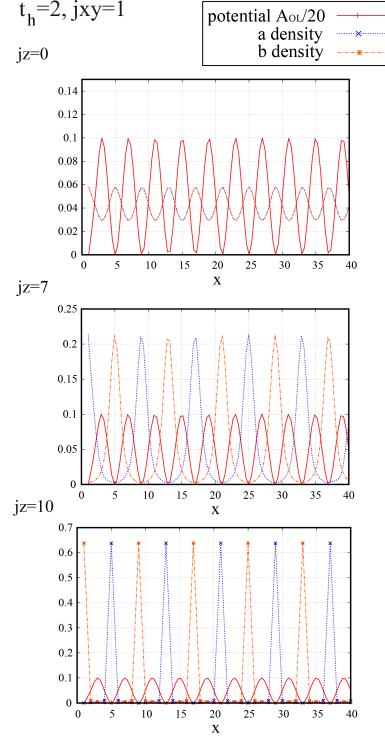


Fig. 2. (Color online) Density profiles of solutions of GP equations. Parameters are $t_h \equiv \frac{\hbar^2}{m} = 2$, $g_{aa} = g_{bb} = 0.5$, $g_{ab} = 0$, and $j_{xy} = 1$. For $j_z = 0$, both a and b -atoms are located in each site of the OL, whereas the CB pattern forms for $j_z = 10$. ℓ is the lattice spacing of the OL and $\ell = 4$ in the numerical calculation.

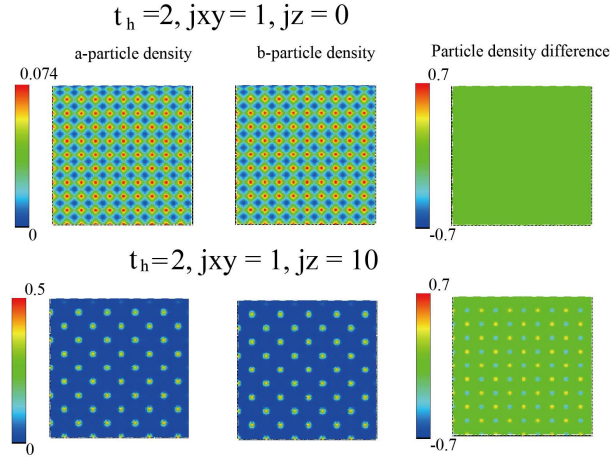


Fig. 3. (Color online) Snapshots of solutions of GP equations, where a -particle density per $(\Delta\ell \times \Delta\ell)$ square = $|\psi_a(x)|^2$, etc. Hopping parameter $t_h \equiv \frac{\hbar^2}{m}$. For $j_z = 0$, the state is homogeneous, whereas the CB solid forms for $j_z = 10$.

The above result indicates that *quantum phase transitions* take place as j_z is increased. It is interesting and also challenging to explore how the quantum phase transition is identified from solutions of the GP equations. As the MC simulation can identify the quantum phase transition by calculating the expectation value of energy and its quantum fluctuations, we

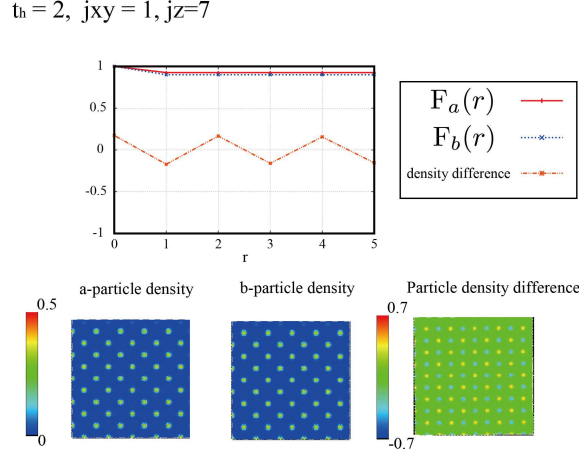


Fig. 4. (Color online) Correlation functions of solutions of GP equations and particle density per $(\Delta\ell \times \Delta\ell)$ square. Both the SF and CB orders exist, i.e., the SS forms for $j_z = 7.0$.

propose to observe similar quantities in solutions of the GP equations. The energy of the state obtained by the GP equations, E_{GP} , is naturally defined as

$$E_{\text{GP}} = \langle H_{\text{GP}}^* \rangle / N_s,$$

$$H_{\text{GP}}^* \equiv H_{\text{GP}} + H_{\text{LR}} - \int d^2x \sum_{\alpha=a,b} \psi_{\alpha}^{\dagger} V_{\text{OL}} \psi_{\alpha}, \quad (17)$$

where N_s is the number of sites of OL and the expectation value is evaluated using the boson wave function that is obtained after a fairly long-time evolution of the GP equations. In the definition of E_{GP} , we subtract the energy of the OL, and therefore E_{GP} corresponds to $\langle H_{\text{EJ}} \rangle$ in the MC simulation.¹²⁾

In Fig.5, the obtained result of E_{GP} is shown as a function of j_z , and this result will be compared with that obtained by the quantum MC simulation in the subsequent subsection. The behavior of E_{GP} in Fig.5 indicates the existence of two phase transitions at $j_z \simeq 6.0$ and 8.0. We verified that a behavior of E_{GP} similar to that shown in Fig.5 is obtained for the solution $\{\psi_a(x), \psi_b(x)\}$ to the GP equation at various times t . We carefully investigated the GP solutions at various j_z values, and verified that, at these two j_z 's, phase transitions from the SF to the SS, and also from the SS to the CB solid take place.

It is interesting to see how the fluctuation of the energy behaves at the above values of j_z . However, the straightforward definition of the specific heat C such as $C = (\langle (H_{\text{GP}}^*)^2 \rangle - \langle H_{\text{GP}}^* \rangle^2) / N_s$ always vanishes when it is evaluated using the wave function $\{\psi_a(x), \psi_b(x)\}$. Then, we define “specific heat” C_{GP} of the present system from the viewpoint of the path-integral formulation of the system. In the path integral, the partition function of system with the

Hamiltonian H is given as

$$Z_H = \int [d\phi] e^{\int d\tau A_c}, \quad \langle H \rangle = \int [d\phi] H e^{\int d\tau A_c} / Z, \quad (18)$$

where action $A_c = (\text{Berry phase}) - H$. Let us assume that there exists a coupling constant g in H , and a phase transition takes place as g is varied. From Eq.(18), the “specific heat” C_g is defined as

$$\begin{aligned} C_g &= \frac{\partial}{\partial g} \langle H \rangle \\ &= \left\langle \frac{\partial H}{\partial g} \right\rangle - \langle H \int d\tau \frac{\partial H}{\partial g} \rangle + \langle H \rangle \left\langle \int d\tau \frac{\partial H}{\partial g} \right\rangle. \end{aligned} \quad (19)$$

Assuming a short-range correlation,

$$\left\langle H \int d\tau \frac{\partial H}{\partial g} \right\rangle - \langle H \rangle \left\langle \int d\tau \frac{\partial H}{\partial g} \right\rangle \propto O(N_s), \quad (20)$$

as the genuine specific heat $\frac{\partial \langle H \rangle}{\partial T} \propto \langle H^2 \rangle - \langle H \rangle^2 \propto O(N_s)$. From the above consideration, we propose to use the following C_{GP} for observing phase transitions:

$$C_{GP} = \left\langle \left(\frac{1}{N_s} \frac{\partial H_{GP}^*}{\partial j_z} - \frac{1}{N_s^2} H_{GP}^* \frac{\partial H_{GP}^*}{\partial j_z} \right) \right\rangle. \quad (21)$$

The calculation of C_{GP} is shown in Fig.6. We again verified that the same behavior of C_{GP} to that shown in Fig.6 is obtained for the solution $\{\psi_a(x), \psi_b(x)\}$ to the GP equation at different times t . C_{GP} has a peak at $j_z \simeq 8.0$ as E_{GP} does. This result seems to indicate that the phase transition from the SS to the CB solid is of second order, whereas that from the 2SF to the SS is a crossover or higher-order phase transition as the derivative of C_{GP} with respect to j_z shows an anomalous behavior at $j_z \simeq 6.0$. This observation will be confirmed by the MC simulations explained in the subsequent subsection.

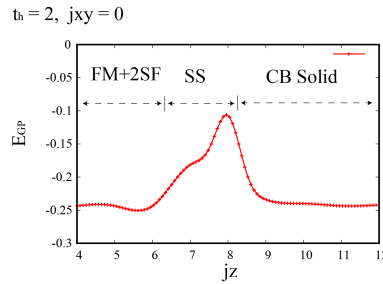


Fig. 5. (Color online) Energy as a function of j_z calculated using the GP equations. The increase in E in the SS state comes from the fact that the hopping term and the j_z -term in the Hamiltonian $H_{GP} + H_{LR}$ compete with each other.

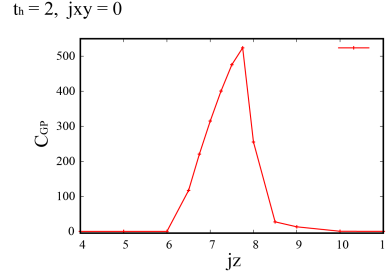


Fig. 6. (Color online) Specific heat as a function of j_z calculated using the GP equations.

3.2 Monte-Carlo simulations: Case of the same mass

In this subsection, we shall study the extended bosonic t-J model H_{EJ} by the MC simulations. We take a_L as the unit of length in the lattice model and will often set $a_L = 1$ in this and subsequent subsections. (Here note that this definition of the unit of length is different from that used in the GP theory, $\Delta\ell = 1$.) For the MC simulations, we also introduce a lattice for the imaginary time τ with the lattice spacing $\Delta\tau$. Then, the model is defined on the three-dimensional (3D) space-time lattice, and we denote the site of the 3D lattice r . The study of the GP equations in the previous subsection strongly suggests that holes are distributed homogeneously except for a very large J_z compared with the hopping parameters t_a and t_b . Therefore, for the practical numerical calculation, we assume a homogeneous distribution of holes and fix the hole density at each site to 30%, i.e., $\rho_{3r} = \rho_3 = 0.3$, as in the GP theory in the previous subsection. Then, we consider the model whose partition function Z_{qXYZ} is given as

$$\begin{aligned} Z_{qXYZ} &= \int \prod_{a=1,2,3} [d\omega_{ar}] [d\lambda_r] e^{A_{qXYZ}}, \\ A_{qXYZ} &= A_\tau + A_L(e^{i\Omega_\sigma}, e^{-i\Omega_\sigma}) + A_z, \end{aligned} \quad (22)$$

where

$$A_\tau = -c_\tau \sum_r \sum_{\sigma=1}^3 \cos(\omega_{\sigma,r+\hat{\tau}} - \omega_{\sigma r} + \lambda_r), \quad (23)$$

$$\begin{aligned} A_L(e^{i\Omega_\sigma}, e^{-i\Omega_\sigma}) &= \sum_{\langle r,r' \rangle_S} \left(C_1 \cos(\Omega_{1,r} - \Omega_{1,r'}) + C_2 \cos(\Omega_{2,r} - \Omega_{2,r'}) \right. \\ &\quad \left. + C_3 \cos(\Omega_{3,r} - \Omega_{3,r'}) \right), \end{aligned} \quad (24)$$

and

$$A_z = -J_z \sum_{\langle r,r' \rangle_S} \Delta\rho_r \Delta\rho_{r'}, \quad \Delta\rho_r \equiv \rho_{1,r} - \rho_{2,r}, \quad (25)$$

where $\langle r, r' \rangle_S$ denotes the NN sites in the 2D spatial lattice. The dynamical variables $\Omega_{a,r}$ ($a = 1, 2, 3$) are related to the phases ω_{ar} as

$$\Omega_{1,r} = \omega_{1r} - \omega_{2r}, \quad \Omega_{2,r} = \omega_{1r} - \omega_{3r}, \quad \Omega_{3,r} = \omega_{2r} - \omega_{3r}.$$

The partition function in Eq.(22) has been derived by integrating out the amplitude modes of the slave-particle fields as explained in Sec.2. Then, the coefficients in the action A_{qXYZ} depend on the density difference $\Delta\rho_r$ and are given as

$$\begin{aligned} c_\tau &= \frac{1}{V_0 \Delta\tau}, \\ C_1 &= J_{xy} \rho_3 \Delta\tau \sqrt{((1 - \rho_3)^2 - (\Delta\rho_r)^2)((1 - \rho_3)^2 - (\Delta\rho_{r'})^2)}, \\ C_2 &= t_a \rho_3 \Delta\tau \sqrt{(1 - \rho_3 + \Delta\rho_r)(1 - \rho_3 + \Delta\rho_{r'})}, \\ C_3 &= t_b \rho_3 \Delta\tau \sqrt{(1 - \rho_3 - \Delta\rho_r)(1 - \rho_3 - \Delta\rho_{r'})}. \end{aligned} \quad (26)$$

From the relation $1/(k_B T) = L \cdot \Delta\tau$, $\Delta\tau$ has dimension $1/(\text{energy})$ and the low-temperature limit is realized for $L \rightarrow \infty$. The parameters c_τ, \sim, C_3 in Eq.(26) are dimensionless, and we put $c_\tau = 2$ for the practical calculation. Then, $k_B T = (c_\tau V_0)/L = 2V_0/L$.

Z_{qXYZ} in Eq.(22) is a functional of $\{\Delta\rho_r\}$, i.e., $Z_{qXYZ} = Z_{qXYZ}(\{\Delta\rho_r\})$. We expect that $\{\Delta\rho_r\}$ behave as variational variables and determine them under the optimal free-energy condition. In the practical calculation, we performed the local update of $\{\Delta\rho_r\}$ by the MC simulation and obtained

$$[Z_{qXYZ}] \equiv \int [d\Delta\rho_r] Z_{qXYZ}(\{\Delta\rho_r\}). \quad (27)$$

However, in the MC calculations, we found that $\{\Delta\rho_r\}$ is *quite stable* for given values of the parameters in the action A_{qXYZ} . This fact indicates that $\{\Delta\rho_r\}$ should be regarded as variational parameters rather than dynamical variables.

In the following, we shall show the results for $\rho_3 = 0.3$ as stated above. For the MC simulations, we employ the grand-canonical ensemble, and therefore, the total numbers of a and b -atoms, N_a and N_b , are *not conserved separately* in each MC update, although $N_a + N_b$ is conserved. We start with the state of the ferromagnetic (FM)+2SF for small $\tilde{J}_z \equiv J_z \Delta\tau$ and increase \tilde{J}_z gradually and see how the phase evolves. For numerical simulations, we employ the standard Monte-Carlo Metropolis algorithm with local update.¹³⁾ The typical sweeps for the measurement is $(30000 - 50000) \times (10 \text{ samples})$, and the acceptance ratio is 40 – 50%. Errors are estimated from 10 samples by the jackknife methods.¹⁴⁾

We first consider the case of the same mass of the a and b -atoms, $t = t_a = t_b = 30/\Delta\tau$. To investigate the phase structure, we calculate the internal energy E_{MC} and specific heat C_{MC} ,

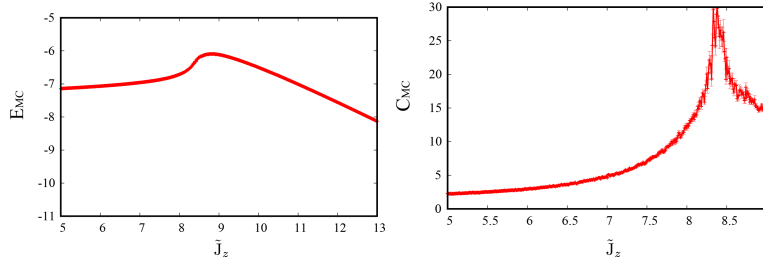


Fig. 7. (Color online) Internal energy and specific heat of qXYZ model as a function of $\tilde{J}_z \equiv J_z \Delta \tau$. Results indicate the existence of the phase transition at $\tilde{J}_z \simeq 8.5$. System size $L = 16$ and $\tilde{J}_{xy} \equiv J_{xy} \Delta \tau = 0.5$.

which are defined as

$$\begin{aligned} E_{MC} &= \langle (A_L + A_z) \rangle / L^3, \\ C_{MC} &= \langle ((A_L + A_z) - E_{MC})^2 \rangle / L^3, \end{aligned} \quad (28)$$

where L is the linear size of the 3D cubic lattice, and we employ the periodic boundary condition. To identify various phases, we also calculate the following pseudo-spin and boson correlation functions:

$$\begin{aligned} G_S(r) &= \frac{1}{L^3} \sum_{r_0} \langle e^{i\Omega_{1,r_0}} e^{-i\Omega_{1,r_0+r}} \rangle, \\ G_a(r) &= \frac{1}{L^3} \sum_{r_0} \langle e^{i\Omega_{2,r_0}} e^{-i\Omega_{2,r_0+r}} \rangle, \\ G_b(r) &= \frac{1}{L^3} \sum_{r_0} \langle e^{i\Omega_{3,r_0}} e^{-i\Omega_{3,r_0+r}} \rangle, \end{aligned} \quad (29)$$

where sites r_0 and $r_0 + r$ are located in the same spatial 2D lattice, i.e., Eqs.(29) are the equal-time correlators. From Eq.(29), $G_S(r)$ measures the FM spin order, whereas $G_a(r)$ and $G_b(r)$ measure the SF (BEC) density of each atom.

The calculations of E_{MC} and C_{MC} shown in Fig.7 clearly indicate the existence of a phase transition at $\tilde{J}_z \simeq 8.5$. The order of the phase transition can be verified by calculating the density of states $N(E)$ that is defined as

$$[Z_{qXYZ}] = \int dE N(E) e^{-E}. \quad (30)$$

We found that $N(E)$ has a single-peak shape for all values of \tilde{J}_z close to the phase boundary. This observation indicates that the phase transition at $\tilde{J}_z \simeq 8.5$ is of second order.

We also measured the correlation functions in Eq.(29) for various \tilde{J}_z values, and show the results in Figs.8 and 9. It is clear that, for $\tilde{J}_z = 5$, the homogeneous superfluid forms. For $\tilde{J}_z = 13$, the CB solid state without the SF LRO appears. However, at $\tilde{J}_z = 8$, the measured correlation functions clearly indicate the existence of the SS, i.e., the density correlation

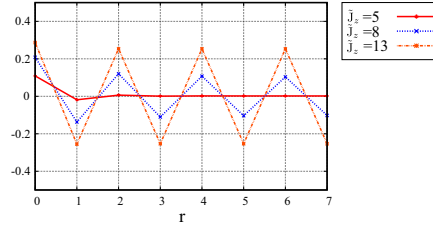


Fig. 8. (Color online) Correlation function of density difference $\Delta\rho_r$. With the results of the correlation functions in Fig.9, it is concluded that there exist three phases.

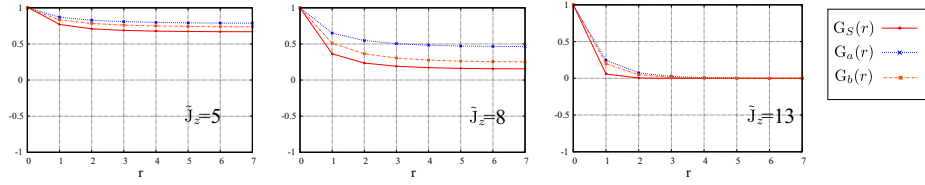


Fig. 9. (Color online) Correlation functions of boson operators defined by Eq.(29). $\tilde{J}_z = J_z \Delta\tau$.

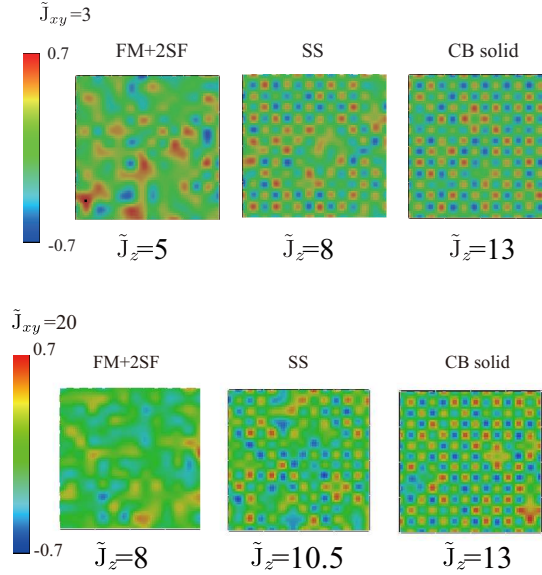


Fig. 10. (Color online) Snapshots of density difference $\Delta\rho_r$ in various phases for $\tilde{J}_{xy} \equiv J_{xy} \Delta\tau = 3$ and 20. The FM+2SF state has a much more homogeneous density for $\tilde{J}_{xy} = 20$ than for $\tilde{J}_{xy} = 3$.

function exhibits the CB diagonal order and the boson correlations also have the SF order. Snapshots of the density difference $\Delta\rho_r$ in various phases are also shown in Fig.10. As the specific heat C_{MC} exhibits no anomalous behavior besides the one at $\tilde{J}_z \simeq 8.5$, which is the phase transition from the SS to the solid, the transition from the SF to the SS must be of higher order or a crossover. This result is in good agreement with the observation using the GP theory given in the previous subsection.

3.3 Monte-Carlo simulations: Case of different masses

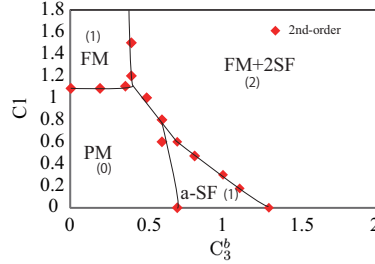


Fig. 11. (Color online) Phase diagram of bosonic t-J model with mass difference $t_a = 2t_b$ and $\tilde{J}_z \ll 1$. $C_3^b \equiv t_b \rho_3 (1 - \rho_3) \Delta \tau / 4$ and $\rho_3 = 0.3$. The numbers in parentheses denote the number of Nambu-Goldstone bosons. This phase diagram was obtained in Ref.8.

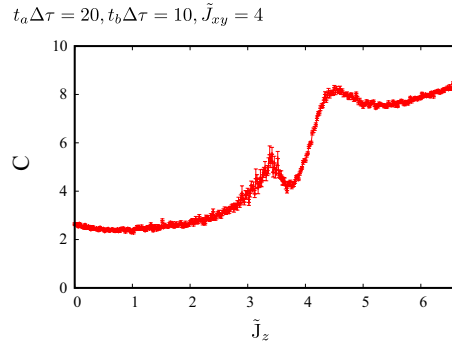


Fig. 12. (Color online) Specific heat C as a function of \tilde{J}_z for the system with mass difference. Other parameters are $t_a \Delta \tau = 20$, $t_b \Delta \tau = 10$, and $\tilde{J}_{xy} = 4$.

Let us turn to the case of the mass difference such as $t_a = 2t_b$. The total filling factor of atoms is 0.7 as in the previous subsections. The phase diagram of that system at $J_z \simeq 0$ was obtained in the previous study.⁸⁾ See Fig.11. In contrast to the same-mass case, there exists a SF state of the a -atom without BEC of the b -atom. (We call it a -SF in Fig.11.) We are particularly interested in how the SF phase of a -atom evolves as \tilde{J}_z is increased. On the other hand for the phase of FM+2SF with $\tilde{J}_z = 0$, we have verified that there appears the SS for intermediate values of \tilde{J}_z and the CB solid for large \tilde{J}_z , as \tilde{J}_z is increased as in the same-mass case.

In Fig.12, we show the specific heat C as a function of \tilde{J}_z for the system with the masses $t_a = 2t_b = 20/\Delta \tau$ and $\tilde{J}_{xy} = 4$. At $\tilde{J}_z = 0$, the system is in the single SF of a -atom. As \tilde{J}_z is increased, there appear a sharp peak at $\tilde{J}_z \simeq 3.3$ and a jump at $\tilde{J}_z \simeq 4.2$. In Fig.13, we show the density correlation function and also snapshot of the density. From the results in Fig.13, the

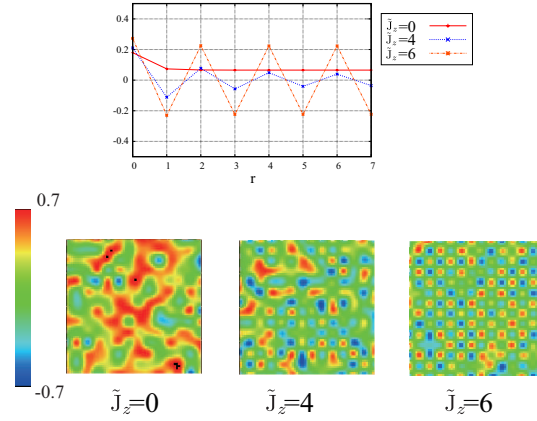


Fig. 13. (Color online) Density correlation and density snapshot for SF of a atom in the system with mass difference.

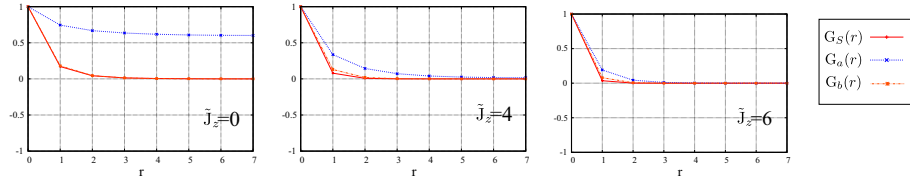


Fig. 14. (Color online) Various correlation functions as a function of \tilde{J}_z in the system with mass difference.

states for $\tilde{J}_z = 0$ and $\tilde{J}_z = 6$ have a homogeneous and CB density, respectively, whereas for $\tilde{J}_z = 4$, only a short-range order of the CB type exists. Furthermore, the correlation functions in Fig.14 show that the state for $\tilde{J}_z = 4$ does not have the SF order, and therefore, it is not a SS. Therefore, the peak at $\tilde{J}_z \simeq 3.3$ in C corresponds to the phase transition from the a -atom SF to the disordered state without any LRO's, whereas the jump at $\tilde{J}_z \simeq 4.2$ corresponds to the transition from the disordered state to the CB solid. The appearance of the disordered state without any LRO's at intermediate \tilde{J}_z stems from the competition of the hopping terms and the pseudospin AF coupling. Note that the nonexistence of the SS in the present case is consistent with the phase diagram of a single-boson system in the square lattice, in which the SS does not form.¹⁵⁾

3.4 Finite-temperature phase transition of the SS and CB solid

In this subsection, we study the finite-temperature phase diagram of the SS. In the previous research,¹⁶⁾ a system of the hard-core boson in a triangular lattice was studied. In that system, a SS forms as a result of competition of the nearest-neighbor repulsion and the hopping amplitude. As the temperature is increased, two phase transitions take place, i.e., at the

first transition, the SF is lost, and at the second one, the solid order is lost. This result was obtained by finite-temperature MC simulations.

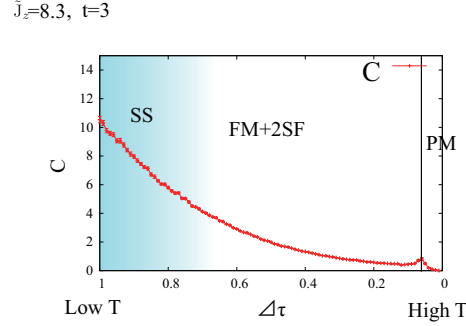


Fig. 15. (Color online) Finite temperature phase diagram. $\tilde{J}_z = J_z \Delta\tau$ and $T \propto 1/\Delta\tau$. PM (paramagnetic) state stands for the disordered state without any orders.

In this subsection, we investigate how the SS, which exists at vanishing (or at very low) temperature, evolves as system temperature is increased. This study is performed by using quantum MC simulations. Temperature of the system T is related to the system size of the imaginary-time direction L_τ and the time slice $\Delta\tau$ as $k_B T = \frac{1}{L_\tau \Delta\tau}$. For the MC simulation, we take L_τ as large as L_s for the linear size of the spatial direction, i.e., $L_\tau = L_s = L$. Then as $\Delta\tau$ is decreased, T becomes higher. As Eq.(26) shows, the coefficients of the action A_{qXYZ} vary with $\Delta\tau$, and the system tends to be quasi-one-dimensional for a small $\Delta\tau$. That is, $J_{xy}\Delta\tau, t\Delta\tau \rightarrow \text{small}$, whereas $\frac{1}{V_0\Delta\tau} \rightarrow \text{large}$. This behavior of the coefficients denotes that the three-dimensional system at low T tends to be one-dimensional for increasing T . Therefore there exists a phase transition from an ordered state to a disordered state as T is increased, as is naturally expected. In particular, it is interesting to see how the two orders of the SS, i.e., the SF and CB solid, disappear as T is increased. More precisely concerning the SF order, the genuine ordered state turns to the state with *quasi-LRO* as the system is quantum 2D at a finite temperature. Therefore, it is expected that a phase transition from the SF to the disordered state belongs to the universality class of the Kosterlitz-Thouless (KT) transition.

We investigated the above problem by the present quantum MC simulations. We consider the same-mass case $t_a = t_b = t$ and the total filling factor 0.7, and focus on the SS observed in Sec. 3.2. The obtained phase diagram is shown in Fig.15. The SS first loses the CB solid order and becomes the FM+2SF state at an intermediate T and then loses the SF order for a higher T . However as the calculation of the specific heat C in Fig.15 indicates, the transition from the SS to FM+2SF has no sharp phase boundary as in the case of the quantum phase transition induced by varying J_z . On the other hand, the transition at $\Delta\tau \simeq 0.06$ exhibits a

small peak in C . This transition is expected to be in the universality class of the KT transition as we explained above. In fact, we verified that the boson correlation functions in the FM+2SF exhibit the quasi-LRO instead of the genuine LRO, whereas those in the PM state decay very rapidly as a function of the distance r .

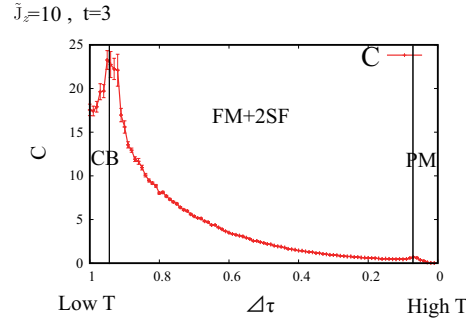


Fig. 16. (Color online) Finite temperature phase diagram of CB solid. At intermediate temperature, the 2SF state appears. $\tilde{J}_z = J_z \Delta\tau$ and $T \propto 1/\Delta\tau$.

Finally, let us turn to the finite-temperature phase diagram of the CB solid. We consider the case of the equal-hopping amplitude again, $t_a = t_b = t$. In Fig.16, we show the finite-temperature phase diagram obtained by the MC simulations. As T is increased, the solid loses the CB order and the SF appears simultaneously. Because of the thermal fluctuations, the effect of the J_z -term is weakened and then a homogeneous state with the SF is realized at an intermediate T . Calculation of the specific heat C in Fig.16 indicates that this phase transition is of second order, although a first-order phase transition is expected as this is a phase transition from the state with the CB order to the state with the SF. The fact that the FM+2SF state has only the quasi-LROs, not the genuine LRO's, probably weakens the phase transition from first to second order. As the temperature increases further, the thermal fluctuations destroy the SF and the state without any orders appears.

4. Conclusion

In this paper, we have studied the two-component cold Bose gas in a square optical lattice. In the strong on-site repulsion case, the system is described by the bosonic t-J model. Using the GP equations and MC simulations, we investigated the phase diagram of the model. In particular, we are interested in how the SF evolves as the coefficient of the J_z -term of the pseudospin interaction is increased. Both the GP theory and the quantum MC simulations show that the SS forms at some critical value of J_z , and then the phase transition from the SS to the CB solid takes place at the second critical value of J_z . This result is consistent with the phase diagram obtained in a previous study.⁸⁾ In the present study, we have not assumed any

density pattern for the boson densities in contrast to our previous analysis.

In the GP theory, we have proposed a method of identifying phase boundaries by calculating the internal energy and “specific heat”. In the MC simulations, we treated the boson densities at each site as variational parameters. The results obtained by the above two methods are in good agreement.

Finally, we studied the finite-temperature phase diagrams of the SS and CB solid, and obtained interesting results, such as, the order of the phase transitions and the appearance of the SF order from the CB solid as the temperature increases.

Acknowledgments

This work was partially supported by Grant-in-Aid for Scientific Research from the Japan Society for the Promotion of Science under Grant No. 23540301.

References

- 1) For reviews, see, e.g., I. Bloch, J. Dalibard, and W. Zwerger, *Rev. Mod. Phys.* **80**, 885 (2008); M. Lewenstein, A. Sanpera, V. Ahufinger, B. Damski, A. S. De, and U. Sen, *Adv. Phy.* **56**, 243 (2008).
- 2) M. Lewenstein, A. Sanpera, and Verònica Ahufinger, *Ultracold atoms in optical lattices: Simulating quantum many-body systems*, (Oxford University Press, Oxford, 2012).
- 3) T. Lahaye, C. Menotti, L. Santos, M. Lewenstein, and T. Pfau, *Rep. Prog. Phys.* **72**, 126401(2009).
- 4) D. Jaksch, C. Bruder, J. I. Cirac, C. W. Gardiner, and P. Zoller, *Phys. Rev. Lett.* **81**, 3108 (1998).
- 5) S. B. Papp, J. M. Pino, and C. E. Wieman, *Phys. Rev. Lett.* **101**, 040402 (2008).
- 6) J. Catani, L. De Sarlo, G. Barrontini, F. Minardi, and M. Inguscio, *Phys. Rev. A* **77**, 011603 (2008).
- 7) Y. Kuno, K. Kataoka, and I. Ichinose, *Phys. Rev. B* **87**, 014518 (2013).
- 8) Y. Kuno, K. Suzuki, and I. Ichinose, *J. Phys. Soc. Jpn.* **82**, 124501(2013).
- 9) M. Boninsegni, *Phys. Rev. Lett.* **87**, 087201 (2001); *Phys. Rev. B* **65**, 134403 (2002); Y. Nakano, T. Ishima, N. Kobayashi, K. Sakakibara, I. Ichinose, and T. Matsui, *Phys. Rev. B* **83**, 235116 (2011); Y. Nakano, T. Ishima, N. Kobayashi, T. Yamamoto, I. Ichinose, and T. Matsui, *Phys. Rev. A* **85**, 023617 (2012).
- 10) GP equation for cold bosonic atomic gases, see for example, M. Tsubota, K. Kasamatsu, and M. Ueda, *Phys. Rev. A* **65**, 023603 (2002).
- 11) As initial states for the numerical evolution of the GP equations, fairly homogeneous states with small fluctuations in amplitude and phase generated by random numbers were prepared.
- 12) We numerically verified that inclusion of the optical lattice term into the energy does not change its qualitative behavior.
- 13) N.Metropolis, A.W.Rosenbluth, M.N.Rosenbluth, A.M.Teller, and E.Teller, *J. Chem. Phys.* **21**, 1087(1953); J. M. Thijssen, *Computational Physics*, (Cambridge University Press, Cambridge, 1999).
- 14) See for example, I.Montvay and G.Muenster, *Quantum Fields on a Lattice*, (Cambridge University Press, Cambridge, 1994).

-
- 15) P. Sengupta, L. P. Pryadko, F. Alet, M. Troyer, and G. Schmid, Phys. Rev. Lett. **94**, 207202 (2005); B. Capogrosso-Sansone, and C. Trefzger, M. Lewenstein, P. Zoller, and G. Pupillo, Phys. Rev. Lett. **104**, 125301 (2010); L. Pollet, J.D. Picon, H.P. Büchler, and M. Troyer, Phys. Rev. Lett. **104**, 125302 (2010);
A. Bühler and H.P. Büchler, Phys. Rev. A **84**, 023607(2011).
- 16) H. Ozawa and I. Ichinose, Phys. Rev. A **86**, 015601(2012).